nature research

https://doi.org/10.1038/s41561-020-0637-7

Supplementary information

Global nitrous acid emissions and levels of regional oxidants enhanced by wildfires

In the format provided by the authors and unedited

Supplementary Information for

Global nitrous acid emissions and regional oxidants levels enhanced by wildfires

This file contains Supplementary Figures S1-S3, Supplementary Tables S1-S8, and Supplementary references.

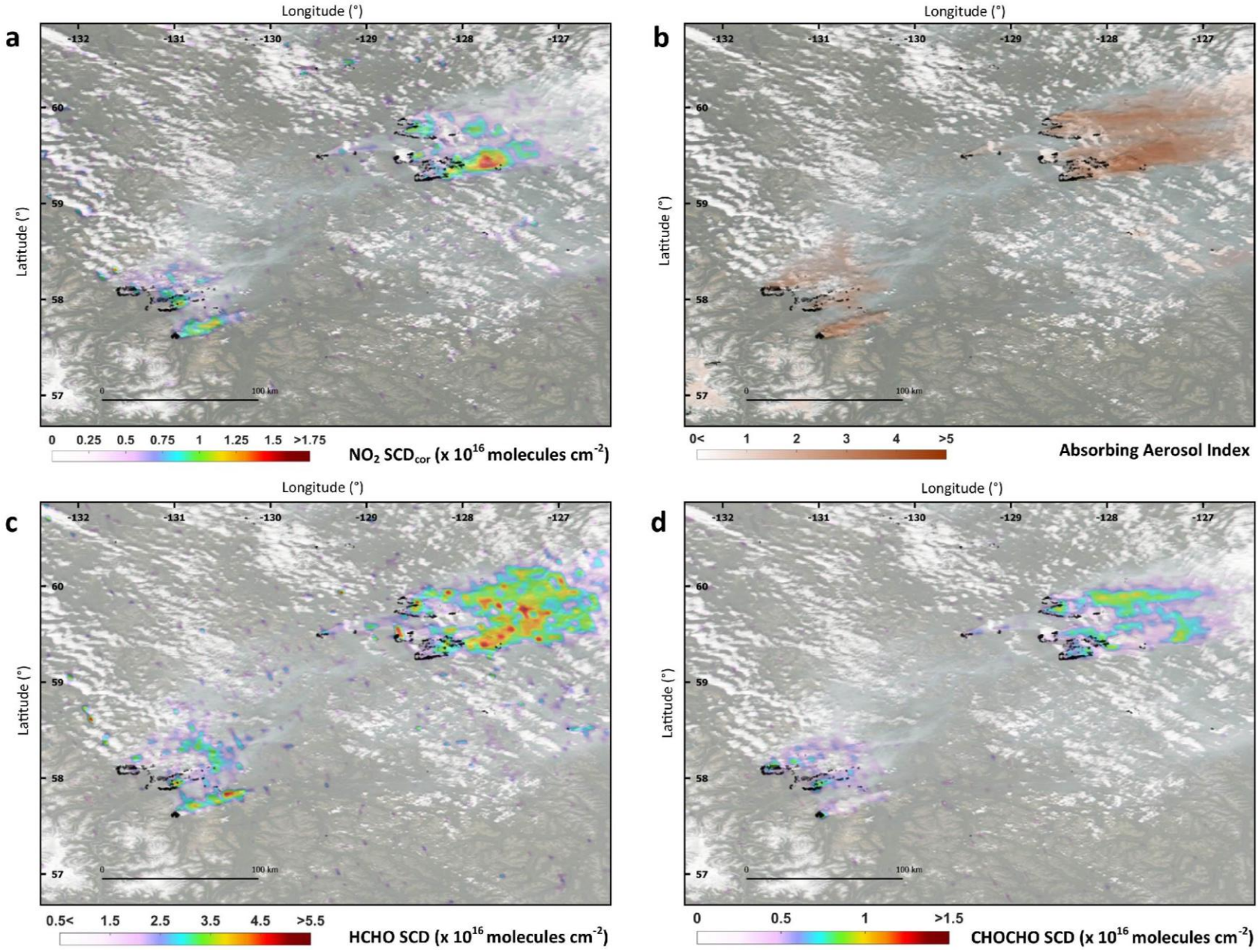
a
Longitude (°)
-132
-131
-130
-129
-128
-127
Latitude (°)
60
59
58
57
0
100 km
0 0.25 0.5 0.75 1 1.25 1.5 >1.75
NO2 SCDcor (x 10^16 molecules cm^-2)
b
Longitude (°)
Latitude (°)
0< 1 2 3 4 >5
Absorbing Aerosol Index
c
Longitude (°)
Latitude (°)
0.5< 1.5 2.5 3.5 4.5 >5.5
HCHO SCD (x 10^16 molecules cm^-2)
d
Longitude (°)
Latitude (°)
0 0.5 1 >1.5
CHOCHO SCD (x 10^16 molecules cm^-2)

Supplementary Fig. 1 | Examples of TROPOMI observations of nitrogen dioxide, absorbing aerosol index, formaldehyde and glyoxal. a, NO_2 slant column densities (corrected for stratospheric NO_2 absorption), for British Columbia on 21 August 2018 (same as Fig. 1a). NO_2 SCDs are retrieved in the same wavelength interval as HONO SCDs. **b**, Absorbing aerosol index (dimensionless) using the wavelength pair 354/388 nm. **c-d**, Formaldehyde and glyoxal slant column densities, respectively. **b-d** are for the same scene as (**a**). The background layers are true-color RGB images with fires detection and thermal anomalies product (black points) from VIIRS/Suomi-NPP instrument (source: https://worldview.earthdata.nasa.gov/), showing smoke aerosols and the fires source locations.

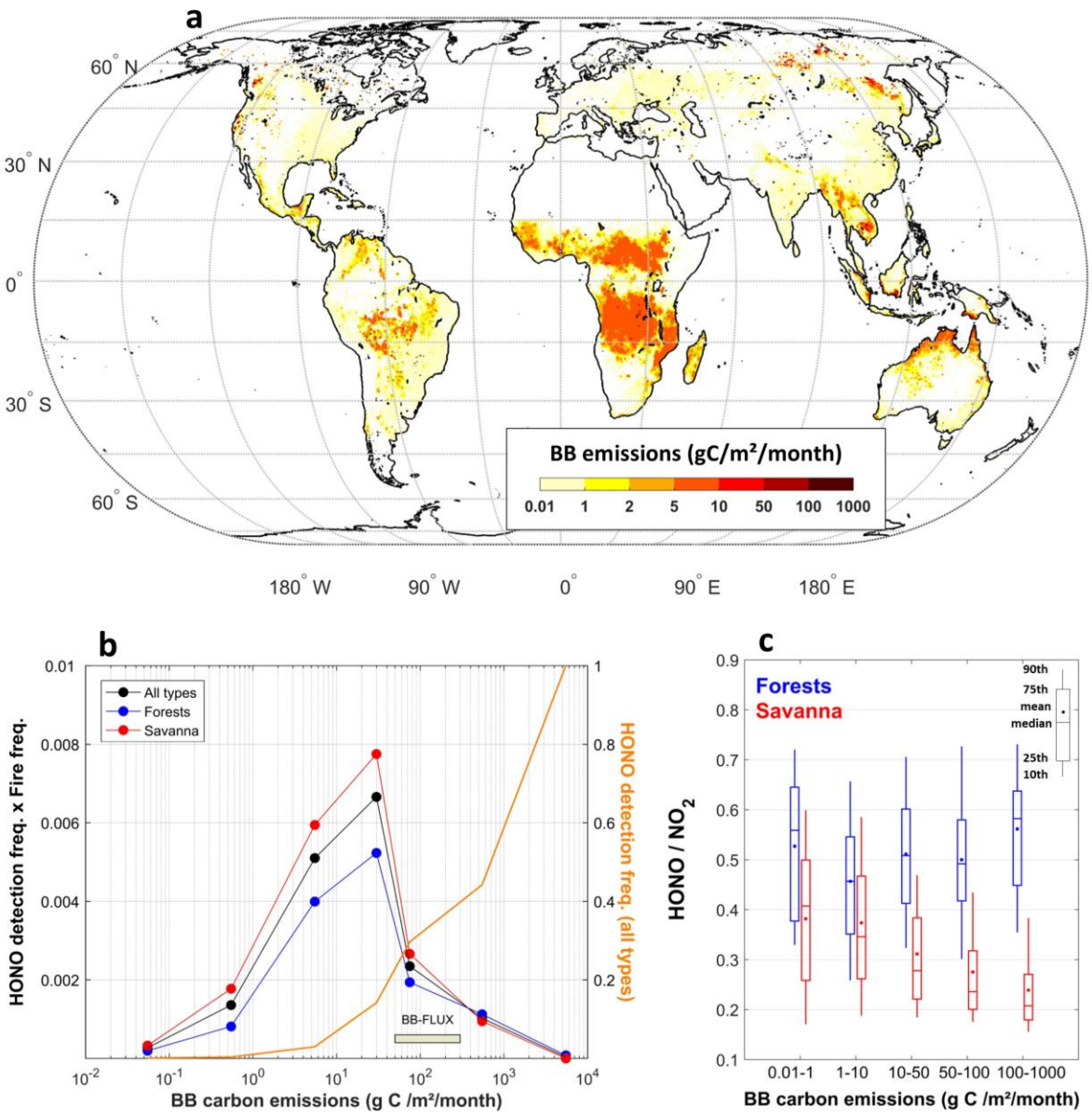

Supplementary Fig. 2 | Global biomass burning carbon emissions, and statistical analysis of TROPOMI HONO detections and HONO/NO_2 with fire activity data. a, Yearly averaged biomass burning carbon emissions from GFED (May 2018-April 2019). **b**, HONO detection frequency multiplied by fire frequency, per bin of carbon emission (monthly averages at 1°x1°), for savanna, forests and both biomes merged, based TROPOMI one-year measurements. HONO detections are mainly found for emissions of 0.5-500 g C/m^2/month; small agriculture fires are not observed. The HONO detection frequency (in orange, for all vegetation types) is estimated, by the fraction of the grids with at least one HONO detection, for a particulate BB carbon emission rate. The pale yellow rectangle gives an indicative range of carbon emissions for the fires during the BB-FLUX campaign. **c**, Whisker plot of RHN for bins of carbon emissions (same as (**b**)), for savanna and forest fires.

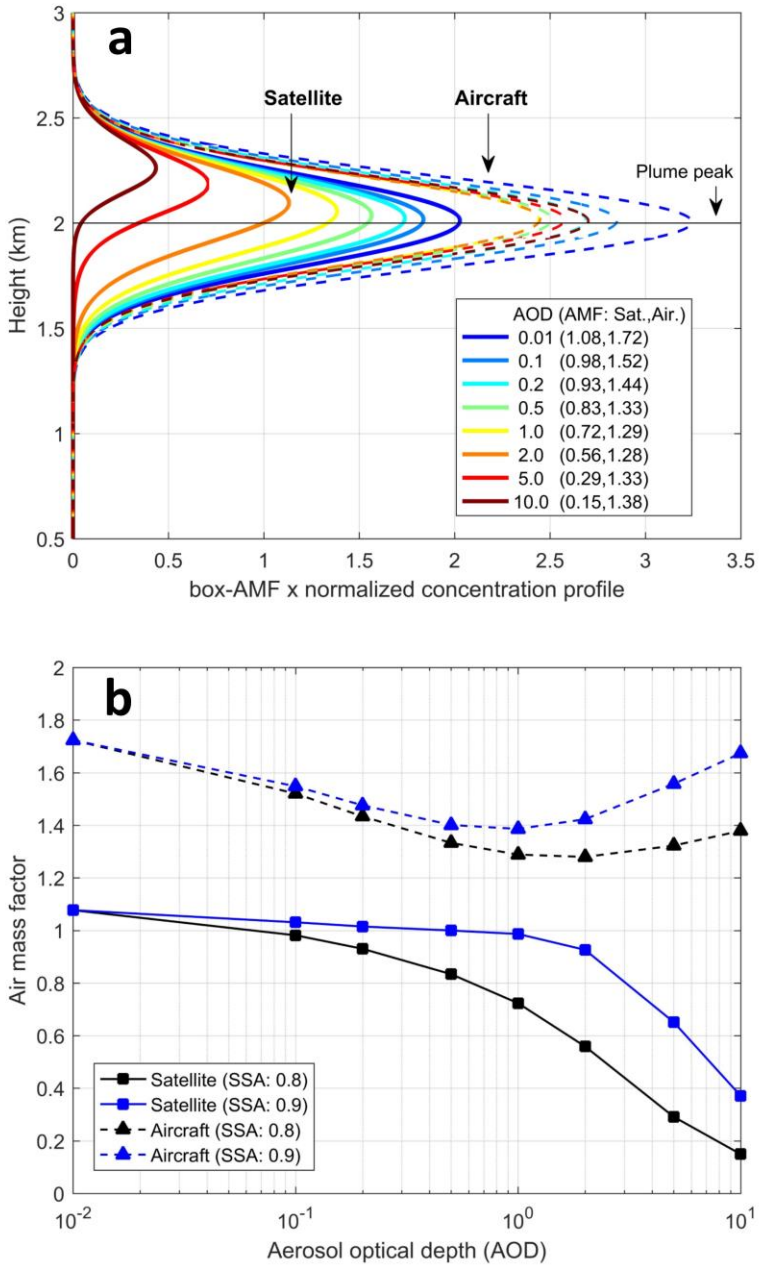

Supplementary Fig. 3 | Illustration of measurement sensitivity change for varying aerosol optical depth for a smoke plume peaking at 2km. a, Height-resolved contribution to the total AMF (Methods) for satellite nadir and aircraft (at 1km flying altitude) zenith-sky viewing geometries, as function of AOD. Satellite and aircraft total AMFs are in the legend. For the satellite geometry, the reduction of sensitivity and shift towards the upper-part of the plume for increasing AOD is clearly visible. Calculations are for clear-sky standard atmosphere, 30° solar zenith angle, 0.05 surface albedo, and typical fresh biomass burning absorbing aerosols with single scattering albedo (SSA) of 0.8. **b,** AMFs for satellite nadir and aircraft zenith-sky viewing geometries, for the same conditions as (**a**), with SSA of 0.8-0.9.

Supplementary Table 1. Summary error budget of NO_2 SCD, HONO SCD and RHN, for satellite and aircraft measurements* used in this study.

	Satellite	Aircraft	Evaluation method - reference
NO_2			
Random error (molec/cm²)	1.8×10^{15}	0.6×10^{15}	Data scatter (1-σ) in clean regions
Random error (%)	12	3	
Absorption cross-section			
Uncertainty (%)	3	3	Vandaele et al. (1998)
Temperature[↓] dep. ± 20K (%)	4	≤4	Behrens et al. (2018)
Systematic error[§] (molec/cm²)	1.3×10^{15}	0.9×10^{15}	Sensitivity tests
Systematic error (%)	9	4	
HONO			
Random error (molec/cm²)	0.7×10^{15}	0.2×10^{15}	Data scatter (1-σ) in clean regions
Random error (%)	9	2	
Absorption cross-section (%)	6	6	Stutz et al. (2000), Gratien et al. (2009)
Systematic error[§] (molec/cm²)	0.8×10^{15}	0.3×10^{15}	Sensitivity tests
Systematic error (%)	11	3	
RHN			
Random error ** (%)	21.2 (40)	5.1	Precision of single measurement
Systematic error ** (%)	26.7 (25)	10.0	Accuracy for comparison with literature
AMF cancellation (%)	1	0.2	AMF calculations over DOAS fit interval[δ]
Comparison total error (%)	25.5	6.9	Accuracy excluding cross-sections errors
Mean relative difference (%) (satellite – aircraft) ± statistical error	+6 ± 8		Figure 2c and Extended Data Figure 1 over plume age intersection

* SCD percent errors given for typical HONO SCDs of 0.75 and 1.0 $\times 10^{16}$ molec/cm², NO_2 SCDs of 1.5 and 2.25 $\times 10^{16}$ molec/cm², for satellite and aircraft observations, respectively.

** Satellite RHN errors vary depending on the observation conditions and retrieved SCDs of HONO and NO_2. An upper limit RHN random error is of 40% for low SCDs. A global estimate of RHN systematic error is of about 25% when accounting for the range of observed SCDs including the conditions with high NO_2 (savanna fires).

[δ] Radiative transfer simulations for varying aerosol optical depth and single scattering albedo (as in Supplementary Fig. S3). Vertical profile shapes of HONO and NO_2 taken identical.

[↓] Difference between plume mean temperature and 294K used in DOAS spectral fitting. The effective plume temperature of the Rabbit Foot fire plume was 277 +- 2 K, and the <4% error is an upper limit.

[§] Mean values derived by varying the settings of the DOAS analysis and SCD background corrections.

Supplementary Table 2. RHNs reported in the literature and in this study, for different types of biomass burning. For each literature study, the results are given as means. The TROPOMI results are classified using MODIS land cover type[1].

	Savanna, grassland, shrubland	Tropical forest	Extra-tropical forest
Field measurements	**0.05 – 0.10**	**0.17 – 0.22**	**0.06 – 0.41 (0.86[δ])**
Trentman et al. (2005)	0.05	-	-
Burling et al. (2011)	0.10 (oak savanna)	-	0.14
Akagi et al. (2012)	-	-	0.17 (chaparral)
Akagi et al. (2013)	-	-	0.27
Bytnerowicz et al. (2016)	-	-	0.06
Müller et al. (2016)	-	-	0.21
Weise et al. (2015)	-	-	0.19
Yokelson et al. (2007)	-	0.17	-
Yokelson et al. (2009)	-	0.22	-
Yokelson et al. (2013)	-	-	0.41 (coniferous canopy)
Peng et al. (2020)	-	-	0.86
Laboratory experiments[§]	**0.05 – 0.19**	**0.17**	**0.13 – 0.20**
Burling et al. (2010)	0.05	-	0.13
Keene et al. (2006)	-	0.17	-
Selimovic et al. (2018)	-	-	0.19
Stockwell et al. (2015)	0.07	-	0.20
Yokelson et al. (2013)	0.19 (semiarid shrubland)	-	-
This study: average ± error*	**0.34±0.08**	**0.41±0.09**	**0.54±0.12**
(10^{th} - 90^{th} percentile)	(0.14 - 0.61)	(0.23 - 0.62)	(0.32 - 0.78)

[δ] Fresh smoke from large wildfires.

[§] NO_2 is assumed in a non-photostationary state for control burns. $HONO/NO_2$ values are calculated for $HONO/NO_x$ molar emission ratios, adapted from reported emission factors (g kg^{-1} of dry matter) of HONO and NO_x (as NO). A fixed NO_x/NO_2 ratio of 1.2 is applied to estimate $HONO/NO_2$ ratios representative of atmospheric measurements of biomass burning plumes[21].

* Systematic uncertainty

Supplementary Table 3. DOAS settings used in this study for TROPOMI retrievals of HONO, NO_2, HCHO and CHOCHO.

HONO and NO_2	
Fitting interval	337-375 nm (TROPOMI band 3)
Cross-sections	HONO 296K (Stutz et al., 2000), NO_2 294K (Vandaele et al., 1998), water vapor (Polyansky et al., 2018), O_2-O_2 293K (Thalman and Volkamer, 2013), O_3 223K and 243K (Serdyuchenko et al., 2014), BrO 223K (Fleischmann et al., 2004), HCHO 298K (Meller and Moortgat, 2000), Ring (Chance and Spurr, 1997)
Polynomial	5th order
Intensity offset	Linear, 1st order
Wavelength shift	1st order
Reference spectrum	Daily radiance (averaged per across-track position) in equatorial Pacific sector (150°E-110°W, 5°S-5°N)
Post-processing	NO_2 SCD stratospheric correction: Latitudinal parameterization (per across-track position) in clean Pacific sector (160°E-150°W)
HCHO	
Fitting interval	328.5-359 nm (TROPOMI band 3)
Cross-sections	HCHO 298K (Meller and Moortgat, 2000), NO_2 220K (Vandaele et al., 1998), O_2-O_2 293K (Thalman and Volkamer, 2013), BrO 223K (Fleischmann et al., 2004), Ring (Chance and Spurr, 1997), O_3 223K and 243K (Serdyuchenko et al., 2014) + Non-linear O_3 absorption effect: 2 pseudo-cross sections from the Taylor expansion of the wavelength and the O_3 optical depth (Puķīte et al., 2010).
Polynomial	5th order
Intensity offset	Linear, 1st order
Wavelength shift	1st order
Reference spectrum	Daily radiance (averaged per across-track position) in equatorial Pacific sector (150°E-110°W, 5°S-5°N)
CHOCHO	
Fitting interval	435-460 nm (TROPOMI band 4)

Cross-sections	CHOCHO (Volkamer et al., 2005), NO_2 220K and 294K (Vandaele et al., 1998), water vapor (Rothman et al., 2013), O_2-O_2 293K (Thalman and Volkamer, 2013), O_3 243K (Serdyuchenko et al., 2014), H_2O liquid (Mason et al., 2016), Ring (Chance and Spurr, 1997)
Polynomial	3rd order
Intensity offset	Linear, 1st order
Wavelength shift	1st order
Reference spectrum	Daily radiance (averaged per across-track position) in equatorial Pacific sector (180°E-120°W, 15°S-15°N)

Supplementary Table S4. VOC photolysis reactions considered as radical sources; OH yield Y_{OH} (assuming NO/NO_2 = 0.2 in biomass burning plumes); ratio of their photolysis rates (radical channel only) relative to that of HCHO, calculated at 30° zenith angle for 300 DU ozone; and relative uncertainty (%) on the product $Y_{OH} \times J_{VOC}$, accounting for uncertainties on the photolysis parameters, based on compilations of experimental data from JPL[32] and IUPAC[33], and on the yield of OH, assuming a 50% error in the conversion of acylperoxy radicals into OH radicals (resulting from a factor of 2 error in the NO to NO_2 ratio).

Reactions	Y_{OH}**(VOC)**	J_{VOC}/J_{HCHO} **(s^{-1} s)**	$\sigma(Y_{OH} \times J_{VOC})$ **(%)**
HCHO → H+HCO	2	1.00	15
CH_3CHO → CH_3+CHO	2	0.146	15
C_2H_5CHO → C_2H_5+CHO	2	0.232	20
C_3H_7CHO → C_3H_7+CHO	2	1.094	30
CH_3COCH_3 → CH_3CO+CH_3	1.3	0.0162	27
$C_2H_5COCH_3$ → $CH_3CO+C_2H_5$	1.3	0.080	60
acrolein → products	0.39	0.030	30
crotonaldehyde → products	2	0.042	30
methacrolein → products	1.51	0.061	100
methylvinylketone → $CH_3CO+CH_2=CH$	1.3	0.066	60
$HOCH_2CHO$ → $CHO+CH_2OH$	2	0.346	30
$HOCH_2COCH_3$ → CH_3CO+CH_2OH	1.3	0.056	50
CHOCHO → 2 CHO	2	2.23	60
CH_3COCHO → CH_3CO+CHO	1.3	4.13	60
$CH_3COCOCH_3$ → 2 CH_3CO	0.6	8.42	100
2-furfural → products	2	0.23	100

Supplementary Table S5. Alkene ozonolysis reactions considered as radical sources; OH yield; reaction rate constant at 286 K; OH production for 1 ppbv VOC at 286 K, with 50 ppbv O_3 and [M]=1.9×10^{19} molec. cm^{-3}, calculated as P_{OH}(VOC+O_3, in pptv h^{-1}) = k(VOC+O_3) × [O_3 in molec. cm^{-3}] × (OH yield) × 3600×10^3; and relative uncertainty (%) on OH production, accounting for uncertainties in the OH yield (assumed equal to 20%) and in the reaction rate constant[34]. OH production from monoterpenes + O_3 depends on speciation (see text). The large uncertainty for monoterpenes σ(P_{OH}(VOC+O_3)) allows for a factor of 3 error on α- to β-pinene ratio in fire plumes.

Reactions	**OH yield**	**k(VOC+O_3)** (10^{-18} **molec.$^{-1}$ cm^3 s^{-1}**)	**P_{OH}(VOC+O_3)** (**pptv h^{-1}**)	**σ(P_{OH}(VOC+O_3))** (**%**)
ethene + O_3	0.26	1.1	1	45
propene + O_3	0.92	7.7	24	55
1-butene + O_3	0.92	8.0	25	40
i-butene + O_3	1.64	9.0	50	35
trans-2-butene + O_3	1.39	160	758	45
cis-2-butene + O_3	1.39	110	521	45
butadiene + O_3	0.29	4.6	46	55
1-pentene + O_3	0.92	10	31	55
1-hexene + O_3	0.92	11	34	55
isoprene + O_3	0.56	9.6	18	35
α-pinene + O_3	1.60	86	469	55
β-pinene + O_3	0.70	16	38	55
monoterpenes + O_3			146	200

Supplementary Table 6. Molar enhancement ratios in biomass burning plumes relative to HCHO[35]. The standard error is given between parentheses, accounting for the standard deviation and number of measurements for each VOC. Those errors might be overestimated given the expected (but not quantified) correlation between Δ(VOC) and Δ(HCHO).

	Δ(VOC)/Δ(HCHO) (mol/mol)			
	savanna	**tropical forests**	**temperate forests**	**boreal forests**
CH_3CHO	0.488(0.126)	0.673(0.476)	0.367(0.059)	0.316(0.045)
C_2H_5CHO	0.022(0.016)	0.022(0.022)	0.022(0.005)	0.071(0.071)
C_3H_7CHO	0.037(0.033)	0.023(0.016)	0.022(0.006)	0.038(0.038)
CH_3COCH_3	0.198(0.029)	0.136(0.136)	0.144(0.031)	0.470(0.183)
$C_2H_5COCH_3$	0.044(0.014)	0.087(0.087)	0.046(0.014)	0.032(0.00)
acrolein	0.209(0.044)	0.145(0.145)	0.088(0.033)	0.101(0.101)
crotonaldehyde	0.087(0.087)	0.043(0.043)	0.082(0.082)	0.105(0.105)
methacrolein	0.045(0.045à	0.025(0.025)	0.027(0.016)	0.024(0.015)
methylvinylketone	0.080(0.080)	0.070(0.070)	0.034(0.010)	0.024(0.017)
$HOCH_2CHO$	0.088(0.034)	0.091(0.091)	0.097(0.097)	0.137(0.137)
$HOCH_2COCH_3$	0.185(0.057)	0.230(0.230)	0.220(0.220)	0.161(0.161)
CHOCHO	0.168(0.168)	0.129(0.129)	0.162(0.162)	0.204(0.204)
CH_3COCHO	0.136(0.096)	0.090(0.090)	0.054(0.054)	0.145(0.145)
$CH_3COCOCH_3$	0.099(0.028)	0.106(0.106)	0.149(0.064)	0.068(0.068)
2-Furfural	0.185(0.108)	0.102(0.102)	0.078(0.046)	0.109(0.109)
Ethane	0.740(0.066)	0.496(0.048)	0.577(0.035)	0.943(0.153)
propene	0.267(0.051)	0.256(0.213)	0.216(0.146)	0.273(0.254)
1-butene	0.036(0.006)	0.016(0.011)	0.031(0.005)	0.049(0.022)
i-butene	0.018(0.003)	0.024(0.024)	0.022(0.006)	0.016(0.006)
trans-2-butene	0.009(0.002)	0.007(0.005)	0.010(0.003)	0.009(0.003)
cis-2-butene	0.007(0.001)	0.007(0.005)	0.010(0.003)	0.007(0.003)

butadiene	0.043(0.007)	0.035(0.035)	0.033(0.005)	0.028(0.005)
1-pentene	0.008(0.001)	0.010(0.010)	0.010(0.002)	0.011(0.003)
1-hexene	0.012(0.002)	0.010(0.010)	0.014(0.002)	0.022(0.022)
isoprene	0.036(0.018)	0.040(0.028)	0.021(0.00)	0.019(0.019)
monoterpenes	0.019(0.008)	0.014(0.014)	0.124(0.069)	0.139(0.139)

Supplementary Table 7. Contribution of VOC photolysis reactions to the production of OH radicals, relative to that of HCHO, based on the yields and rates of Supplementary Table 4 and on the enhancement ratios of Supplementary Table 6. The estimated uncertainty is given within parentheses.

	$P_{OH}(VOC)/P_{OH}(HCHO)$ (pptv h^{-1} $pptv^{-1}$ h)			
	savanna	**tropical forests**	**temperate forests**	**boreal forests**
CH_3CHO	0.071(0.029)	0.098(0.084)	0.054(0.017)	0.046(0.013)
C_2H_5CHO	0.005(0.005)	0.005(0.006)	0.005(0.002)	0.016(0.019)
C_3H_7CHO	0.040(0.048)	0.025(0.025)	0.024(0.014)	0.042(0.055)
CH_3COCH_3	0.002(0.001)	0.001(0.001)	0.001(0.001)	0.004(0.003)
$C_2H_5COCH_3$	0.002(0.002)	0.004(0.006)	0.002(0.002)	0.002(0.001)
acrolein	0.001(0.001)	0.001(0.001)	0.001(0.001)	0.001(0.001)
crotonaldehyde	0.004(0.005)	0.002(0.003)	0.003(0.004)	0.004(0.005)
methacrolein	0.002(0.004)	0.001(0.002)	0.001(0.002)	0.001(0.002)
methylvinylketone	0.003(0.005)	0.003(0.005)	0.001(0.001)	0.001(0.001)
$HOCH_2CHO$	0.030(0.021)	0.031(0.040)	0.034(0.044)	0.047(0.061)
$HOCH_2COCH_3$	0.007(0.006)	0.008(0.012)	0.008(0.012)	0.006(0.009)
CHOCHO	0.375(0.600)	0.288(0.461)	0.361(0.578)	0.455(0.728)
CH_3COCHO	0.365(0.32)	0.242(0.387)	0.145(0.232)	0.389(0.622)
$CH_3COCOCH_3$	0.250(0.321)	0.268(0.536)	0.376(0.538)	0.172(0.344)
2-Furfural	0.043(0.068)	0.023(0.046)	0.018(0.029)	0.025(0.050)
ALL except CHOCHO	0.825(0.48)	0.71(0.67)	0.67(0.59)	0.76(0.72)

Supplementary Table 8. Contribution of VOC ozonolysis reactions to the production of OH radicals calculated for 50 ppbv O_3 at 286 K, based on the molar enhancement ratios of Supplementary Table 6, for 1 ppbv HCHO and [M]=1.9 10^{19} molec. cm^{-3}. The uncertainties (accounting for uncertainties in ozonolysis rates and yields, and in the molar enhancements in fire plumes) are given within parentheses.

	P_{OH}(VOC) (pptv h^{-1})			
	savanna	**tropical forests**	**temperate forests**	**boreal forests**
ethene	0.72(0.39)	0.49(0.27)	0.57(0.29)	0.93(0.57)
propene	6.44(.77)	6.18(8.54)	5.21(6.39)	6.59(9.76)
1-butene	0.91(0.52)	0.40(0.44)	0.78(0.44)	1.23(1.04)
i-butene	0.45(0.03)	0.61(0.82)	0.55(0.3)	0.40(0.29)
trans-2-butene	6.82(4.58)	5.31(6.18)	7.58(5.69)	6.82(5.34)
cis-2-butene	3.66(2.17)	3.66(4.26)	5.21(3.91)	3.66(3.22)
butadiene	1.95(1.39)	1.59(2.46)	1.50(1.05)	1.27(0.93)
1-pentene	0.36(0.24)	0.45(0.70)	0.45(0.34)	0.49(0.40)
1-hexene	0.28(0.20)	0.34(0.53)	0.49(0.34)	0.76(1.18)
isoprene	0.66(0.69)	0.74(0.93)	0.38(0.28)	0.34(0.53)
monoterpenes	2.80(6.78)	2.05(6.15)	18.1(46.2)	20.3(60.9)
ALL	25.1(9.9)	21.8(13.3)	40.8(47.2)	42.8(62.1)

Supplementary references

1. Friedl, M. A. et al. MODIS Collection 5 global land cover: algorithm refinements and characterization of new datasets. *Remote Sens. Environ.* **114**, 168–182 (2010).
2. Peng, Q., et al. HONO Emissions from Western U.S. Wildfires Provide Dominant Radical Source in Fresh Wildfire Smoke. *Environ. Sci. Technol*. **54**, 5954-5963 (2020).
3. Vandaele, A. C. et al. Measurements of the NO2 absorption cross section from 42 000cm−1 to 10 000cm−1 (238–1000 nm) at 220K and 294 K. *J. Quant. Spectrosc. Ra.* **59**, 171–184 (1998).
4. Behrens, L. K. et al. GOME-2A retrievals of tropospheric NO2 in different spectral ranges – influence of penetration depth. *Atmos. Meas. Tech.* **11**, 2769-2795 (2018).
5. Stutz, J. et al. UV-vis Absorption Cross-Section of Nitrous Acid. *J. Geophys. Res.* **105**, 14585–14592 (2000).
6. Gratien, A. et al. Experimental intercomparison of the absorption cross-sections of the nitrous acid (HONO) in the ultraviolet and mid-infrared spectral regions. *Journal of Quantitative Spectroscopy and Radiative Transfer.* **110**, 256-263 (2009).
7. Trentmann, J. et al. An analysis of the chemical processes in the smoke plume from a savanna fire. *J. Geophys. Res.* **110**, D12301 (2005).
8. Burling, I. R. et al. Airborne and ground-based measurements of the trace gases and particles emitted by prescribed fires in the United States. *Atmos. Chem. Phys.* **11**, 12,197–12,216 (2011).
9. Akagi, S. K. et al. Evolution of trace gases and particles emitted by a chaparral fire in California. *Atmos. Chem. Phys.* **12**, 1397-1421 (2012).
10. Akagi, S. K. et al. Measurements of reactive trace gases and variable O_3 formation rates in some South Carolina biomass burning plumes. *Atmos. Chem. Phys.* **13**, 1141-1165 (2013).
11. Bytnerowicz, A. et al. Ground-level air pollution changes during a boreal wildland mega-fire. *J. Sci. tot. Environ.* **572**, 755-769 (2016).
12. Müller, M. et al. In situ measurements and modeling of reactive trace gases in a small biomass burning plume. *Atmos. Chem. Phys.* **16**, 3813-3824 (2016).
13. Weise, D. R., Johnson, T. J., Reardon, J. Particulate and trace gas emissions from prescribed burns in southeastern U.S. fuel types: Summary of a 5-year project. *Fire Safety Journal.* **74**, 71-81 (2015).
14. Yokelson, R. J. et al. The Tropical Forest and Fire Emissions Experiment: overview and airborne fire emission factor measurements. *Atmos. Chem. Phys.* **7**, 5175-5196 (2007).
15. Yokelson, R. J. et al. Emissions from biomass burning in the Yucatan. *Atmos. Chem. Phys.* **9**, 5785–5812 (2009).
16. Yokelson, R. J. et al. Coupling field and laboratory measurements to estimate the emission factors of identified and unidentified trace gases for prescribed fires. *Atmos. Chem. Phys.* **13**, 89-116 (2013).

17. Burling, I. R. et al. Laboratory measurements of trace gas emissions from biomass burning of fuel types from the southeastern and southwestern United States. *Atmos. Chem. Phys.* **10**, 11115-11130 (2010).
18. Keene, W. C. et al. Emissions of major gaseous and particulate species during experimental burns of southern African biomass. *J. Geophys. Res.* **111**, D04301 (2006).
19. Selimovic, V. et al. Aerosol optical properties and trace gas emissions by PAX and OP-FTIR for laboratory-simulated western US wildfires during FIREX. *Atmos. Chem. Phys.* **18**, 2929-2948 (2018).
20. Stockwell, C. E., Veres, P. R., Williams, J., Yokelson, R. J. Characterization of biomass burning emissions from cooking fires, peat, crop residue, and other fuels with high-resolution proton-transfer-reaction time-of-flight mass spectrometry. *Atmos. Chem. Phys.* **15**, 845-865 (2015).
21. Simpson, I. J. et al. Boreal forest fire emissions in fresh Canadian smoke plumes: C1-C10 volatile organic compounds (VOCs), CO_2, CO, NO_2, NO, HCN and CH_3CN. *Atmos. Chem. Phys.* **11**, 6445-6463 (2011).
22. Polyansky, O. L. et al. Exomol molecular line lists XXVI: a complete high accuracy line list for water. *Mon. Not. R. Astron. Soc.* **480**(2), 2597–2608 (2018).
23. Thalman, R. M., Volkamer, R. Temperature Dependent Absorption Cross-Sections of O_2-O_2 collision pairs be- tween 340 and 630nm and at atmospherically relevant pressure. *Phys. Chem. Chem. Phys.* **15**, 15371–15381 (2013).
24. Serdyuchenko, A., Gorshelev, V., Weber, M., Chehade, W., Burrows, J. P. High spectral resolution ozone absorption cross-sections – Part 2: Temperature dependence. *Atmos. Meas. Tech.* **7**, 625–636 (2014).
25. Fleischmann, O. C., Hartmann, M., Burrows, J.P., Orphal, J. New ultraviolet absorption cross-sections of BrO at atmospheric temperatures measured by time-windowing Fourier transform spectroscopy. *J. Photochem. Photobiol. A.* **168**, 117–132 (2004).
26. Meller, R., Moortgat, G. K. Temperature dependence of the absorption cross section of HCHO between 223 and 323 K in the wavelength range 225–375 nm. *J. Geophys. Res.* **105**, 7089–7102 (2000).
27. Chance, K., Spurr, R. J. Ring effect studies: Rayleigh scattering including molecular parameters for rotational Raman scattering, and the Fraunhofer spectrum. *Appl. Optics*. **36**, 5224–5230 (1997).
28. Puķīte, J., Kühl, S., Deutschmann, T., Platt, U., Wagner, T. Extending differential optical absorption spectroscopy for limb measurements in the UV. *Atmos. Meas. Tech.* **3**, 631–653 (2010).
29. Volkamer, R., Spietz, P., Burrows, J.P., Platt, U. High-resolution absorption cross-section of glyoxal in the UV-vis and IR spectral ranges. *J. Photochem. Photobiol. A: Chemistry.* **172**(1), 35–46 (2005).
30. Rothman, L. S. et al. The HITRAN 2012 molecular spectroscopic database. *Journal of Quantitative Spectroscopy and Radiative Transfer.* **130**, 4–50 (2013).
31. Mason, J. D., Cone, M. T., Fry, E. S. Ultraviolet (250–550 nm) absorption spectrum of pure water. *Appl. Optics. Optical Society of America*, **55**(25), p. 7163. (2016).

32. Burkholder, J. B. et al. Chemical Kinetics and Photochemical Data for Use in Atmospheric Studies. Jet Propulsion Laboratory (JPL), California Institute of Technology, Pasadena, California. http://jpldataeval.jpl.nasa.gov (2015).
33. Atkinson, R. et al. Evaluated kinetic and photochemical data for atmospheric chemistry: volume I - Gas phase reactions of O_x, HO_x, NO_x, and SO_x species. *Atmos. Chem. Phys.* **4**, 1461-1738 (2004). http://iupac.pole-ether.fr/),
34. Atkinson, R. et al. Evaluated kinetic and photochemical data for atmospheric chemistry: Volume II – gas phase reactions of organic species. *Atmos. Chem. Phys.* **6**, 3625-4055 (2006).
35. Andreae, M. O. Emissions of trace gases and aerosols from biomass burning – An updated assessment. *Atmos. Chem. Phys.* **19***,* 8523-8546 (2019).